Chinese Chemical Letters 37 (2026) 110590

Contents lists available at ScienceDirect

Chinese Chemical Letters

journal homepage: www.elsevier.com/locate/cclet

1D COFs with phthalocyanine functional building blocks and imide linkage for superior electrocatalytic nitrate reduction

Mingrun Li[a], Bin Han[a,*], Lei Gong[b], Yucheng Jin[a], Mingyue Wang[a], Xu Ding[a], Dongdong Qi[a], Jianzhuang Jiang[a,*]

[a] Beijing Advanced Innovation Center for Materials Genome Engineering, Beijing Key Laboratory for Science and Application of Functional Molecular and Crystalline Materials, Department of Chemistry and Chemical Engineering, School of Chemistry and Biological Engineering, University of Science and Technology Beijing, Beijing 100083, China
[b] National University of Singapore (Suzhou) Research Institute, Suzhou 215123, China

ARTICLE INFO

Article history:
Received 19 September 2024
Revised 17 October 2024
Accepted 29 October 2024
Available online 30 October 2024

Keywords:
One-dimensional
Covalent organic framework
Phthalocyanine
Nitrate reduction
Electrocatalysis

ABSTRACT

In comparison with their 2D and 3D counterparts, 1D covalent organic frameworks (COFs) have rarely been investigated due to the synthetic challenge arising from the strict necessary matching in the molecular symmetry between corresponding building blocks and linking units in addition to the unmanageable packing of 1D organic chains once formed. Herein, two novel imide-linked 1D COFs with phthalocyanine building blocks, namely NiPc-CZDM-COF and NiPc-CZDL-COF, were fabricated from the hydrothermal synthesis reaction of 2,3,9,10,16,17,23,24-octacarboxyphthalocyaninato nickel(II) (NiPc$(COOH)_8$) with 9*H*-carbazole-3,6-diamine (CZDM) and 4,4′-(9*H*-carbazole-3,6-diyl)dianiline (CZDL), respectively. Two COFs have high crystallinity on the basis of powder X-ray diffraction analysis and high-resolution transmission electron microscopy. Due to their high ratio of exposed active centers on the edge sites of porous ribbons, both NiPc-CZDM-COF and NiPc-CZDL-COF electrodes display high utilization efficiency of NiPc electroactive sites of 8.0 % and 7.5 % according to the electrochemical measurement, resulting in their excellent capacity toward electrocatalytic nitrate reduction with the nitrate-to-NH_3 Faradaic efficiency of nearly 100 %. In particular, NiPc-CZDM-COF electrode exhibits superior electrocatalytic performance with high NH_3 partial current density of $-246\ mA/cm^2$, ammonia yield rate of 19.5 mg cm^{-2} h^{-1}, and turnover frequency of $5.8\ s^{-1}$ at -1.2 V in an H-type cell associated with its higher conductivity. This work reveals the good potential of 1D porous crystalline materials in electrocatalysis.

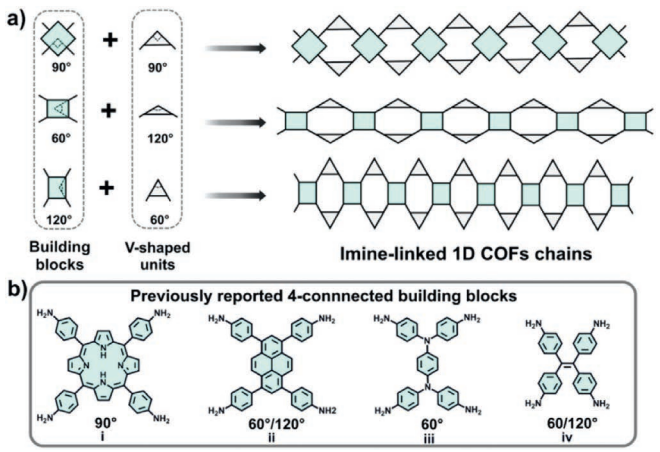
© 2025 Published by Elsevier B.V. on behalf of Chinese Chemical Society and Institute of Materia Medica, Chinese Academy of Medical Sciences.

Covalent organic frameworks (COFs) composed of organic building units *via* covalent bonds have been widely used for gas storage and separation [1–4], energy storage [5–10], catalysis [11–14], and optoelectronics [15–19]. Diverse COFs have been guided and fabricated according to the predesigned topology diagram based on the connectivity and geometry of discrete organic building units [20–28]. Different from their two-dimensional (2D) and three-dimensional (3D) counterparts, one-dimensional (1D) COFs are conventionally constructed from four connected planar aromatic building blocks and nonlinear V-shaped C_2 linking units, under the condition that the sum of the angle between two neighboring connecting sites in the building block and the angle of the V-shaped linking unit amounts to 180°, along one dimension to form 1D chain (Scheme 1a) [29]. This chain in turn aggregates each other on the basis of van der Waals force, π-π interaction, and/or hydrogen bonds to form 1D porous ribbon. As easily expected, the relatively weak interaction between 1D chains usually leads to extremely high anisotropy and entropy-driven random packing, resulting in the difficulty in the fabrication of 1D COFs [30]. As a consequence, only about 20 examples of 1D COFs with building blocks limited to porphyrin, tetraphenyl ethylene, bis(triphenylamine), and pyrene skeletons and linkage limited to reversible imine bonds have been isolated and reported since 2020 [31–34] to the best of our knowledge (Scheme 1b). For the purpose of extending the structure and functionality diversity, more 1D COFs with different building clocks, linking units, and in particular new linkages other than imine bonds are highly desired in this field.

Ammonia (NH_3), as an irreplaceable chemical material, has been widely utilized in industry [35]. Thus far the industrial NH_3

* Corresponding authors.
E-mail addresses: hanbin@ustb.edu.cn (B. Han), jianzhuang@ustb.edu.cn (J. Jiang).

https://doi.org/10.1016/j.cclet.2024.110590
1001-8417/© 2025 Published by Elsevier B.V. on behalf of Chinese Chemical Society and Institute of Materia Medica, Chinese Academy of Medical Sciences.



Scheme 1. Schematic structures of (a) building blocks, V-shaped linking units, and (b) topological structures of 1D imine-linked COFs reported thus far.

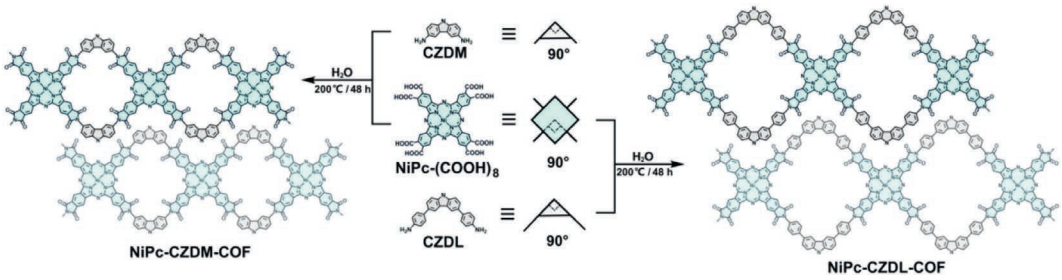
production has still been dominated by the energy-consuming Haber-Bosch process [36]. The eco-friendly electrochemical NH_3 synthesis is expected to play important role in future NH_3 production [37]. However, electrochemical nitrogen reduction reaction (NRR) is unsatisfactory due to the low solubility of N_2 in electrolyte and high dissociation energy of N≡N bonds (941 kJ/mol) [38]. As a consequence, the more efficient electrochemical nitrate reduction reaction (NO_3RR) associated with the easily dissolved NO_3^- and easier breaking of N=O bonds (204 kJ/mol) has attracted increasing attention and widely investigated in recent years [39,40], leading to the development of diverse NO_3RR electrocatalysts including metal nanoparticles [41], alloys [42], metal oxides [43], single-atom catalysts (SACs) [44], and metal-organic frameworks (MOFs) [45]. However, the high cost and unsatisfactory energy conversion efficiency of inorganic electrocatalysts and relatively low stability of MOFs-based electrocatalysts, to some degree, hinder their potential practical applications [46,47]. Fortunately, more robust COFs linked by covalent bonds have been revealed to exhibit excellent performance for diverse electrocatalytic reactions like carbon dioxide reduction reaction [48–51], H_2O_2 synthesis [52,53], and oxygen reduction reaction [54–56]. Quite lately, the NO_3RR functionality of a few 2D COFs has been explored. In 2023, a nickel porphyrin-based 2D COF was revealed to show electrocatalytic NO_3RR performance with the nitrate-to-NH_3 Faradaic efficiency (FE_{NH_3}) of ~90% and NH_3 production rate of 2.5 mg cm^{-2} h^{-1} [57]. This was followed by the utilization of an iron porphyrin-based 2D COF with the FE_{NH_3} of 85.4% and NH_3 yield rate of 2.88 mg cm^{-2} h^{-1} [58]. Also in the same year, a 2D metal-COF nanosheet was constructed for this process with the FE_{NH_3} of 85.4% and NH_3 yield rate of 8.52 mg cm^{-2} h^{-1} [59]. It is noteworthy that the active sites available of 2D COFs are usually very low owing to the inaccessible catalytic centers in their buried layers. 1D COFs possessing high ratio of exposed active centers on the edge sites of porous ribbons containing finite 1D chains are therefore expected to favor the electrocatalysis.

Inspired by the efficient electrocatalysis performance of molecular phthalocyanine compounds for NO_3RR, two unprecedented phthalocyanine-based 1D COFs with imide-linkage, namely NiPc-CZDM-COF and NiPc-CZDL-COF, were designed and synthesized by the imidization reaction of tetra-connected 2,3,9,10,16,17,23,24-octacarboxyphthalocyaninato nickel(II) (NiPc-$(COOH)_8$) with V-shaped C_2 linking units of 9*H*-carbazole-3,6-diamine (CZDM) and 4,4′-(9*H*-carbazole-3,6-diyl)dianiline (CZDL), respectively (Scheme 2). Both 1D COFs possess high crystallinity and AA stacking manners according to high-resolution transmission electron microscopy (HRTEM) photos. Both of them display excellent electrocatalytic NO_3RR activity owing to the utilization of high ratio of exposed catalytic sites on the edge sites of finite 1D chains in every porous ribbon. Particularly, NiPc-CZDM-COF electrode shows the superior electrocatalytic performance associated with its high conductivity revealed by current−voltage curves with FE_{NH_3} of ~100%, record-breaking NH_3 current density (j_{NH_3}) of −246 mA/cm^2 in MOFs- and COFs-based electrocatalysts, and ammonia yield rate of 19.5 mg cm^{-2} h^{-1} at −1.2 V. The present result not only provides a good catalyst for efficient electrocatalytic NO_3RR but also unveils the great potential of 1D porous COFs for diverse electrocatalysis reactions.

Two polyimide-linked phthalocyanine-based 1D COFs were prepared by the hydrothermal imidization reaction of NiPc$(COOH)_8$ with CZDM and CZDL, respectively (Scheme 2). In contrast to previous reports on synthesizing polyimide COFs with anhydride derivatives as building blocks and using isoquinoline as catalyst for >5 days in organic solvent [60,61], in the present case the green hydrothermal synthesis using H_2O as solvent takes only 2 days, affording the 1D COFs in high yield over 90%. As shown in the fourier transform infrared (FT-IR) spectroscopy (Fig. S1 in Supporting information), the absence of amino band of CZDM and CZDL at about 3350 cm^{-1}, the vanished O–H stretching vibration at *ca.* 3040 cm^{-1} and CO peaks at *ca.* 1712 cm^{-1} of NiPc$(COOH)_8$, and the newly appeared C=O signal at *ca.* 1766 and 1708 cm^{-1} and pristine C–N–C signal at *ca.* 1364 cm^{-1} indicate the successful polymerization between NiPc$(COOH)_8$ and CZDM/CZDL. The Ni contents were measured as 4.04% and 4.03% in NiPc-CZDM-COF and NiPc-CZDL-COF, respectively, based on the inductively coupled plasma optical emission spectrometer. Thermal gravimetric analysis discloses that two COFs can keep their structure over 500 °C, indicating their good thermal stability (Figs. S2 and S3 in Supporting information).

The highly crystalline structures of both COFs were analyzed by means of PXRD analysis combined with computational simulation (Figs. 1a and d). In consideration of the nonlinear topology of CZDM and CZDL, the possible structure models of 1D AA and 1D AB stacking models were built for two COFs. Take NiPc-CZDM-COF as an example, the experimental PXRD pattern matches well with the AA stacking model rather than AB stacking model (Figs. S4 and S5 in Supporting information). On the help of Pawley refinement, NiPc-CZDM-COF has the unit cell parameters of $a = 41.91$ Å, $b = 21.87$ Å, $c = 3.33$ Å, and $\alpha = \beta = \gamma = 90°$ with $R_p = 2.12\%$ and $R_{wp} = 2.75\%$. The intense diffraction peaks at *ca.* 2θ 4.51°, 7.62°, 11.73°, and 26.71° can be assigned to the (110), (310), (420), and (001) planes. For NiPc-CZDL-COF, the 1D AA stacking model is also disclosed in a similar manner (Figs. S6 and S7 in Supporting information). The unit cell parameters of $a = 46.74$ Å, $b = 27.42$ Å, $c = 3.31$ Å, and $\alpha = \beta = \gamma = 90°$ with $R_p = 2.61\%$ and $R_{wp} = 3.36\%$ can also be obtained. The four obvious diffraction peaks sitting at *ca.* 2θ of 3.73°, 6.42°, 9.89°, and 27.02° belong to the (110), (310), (420), and (001) planes. The pore sizes of NiPc-CZDM-COF and NiPc-CZDL-COF were measured to be 14.7 and 21.0 Å, respectively, substantially consistent with those deduced from HRTEM photos and BET measurements as depicted below. In addition, the distance of adjacent chains compiled together *via* $\pi-\pi$ interactions is revealed to be 0.33 nm for both COFs (Figs. 1b, c, e, and f).

Transmission electron microscope (TEM) and scanning electron microscope (SEM) photos manifest the nano-ribbon shaped morphology with the diameter of 30–60 nm for both COFs (Figs. S8-S11 in Supporting information). The HRTEM photos disclose the well-aligned lattice fringes of (001) crystal face with π-π stacking distance of 0.33 nm and the well aligned pore structure with the pore sizes of 14.5 and 21.3 Å for NiPc-CZDM-COF and NiPc-CZDL-COF, respectively (Figs. 1g-i, Figs. S12 and S13 in Supporting information), basically consistent with those derived from structural models and BET measurement. Uniformly distribution of C, N, O,



Scheme 2. Schematic synthesis of NiPc-CZDM-COF and NiPc-CZDL-COF.

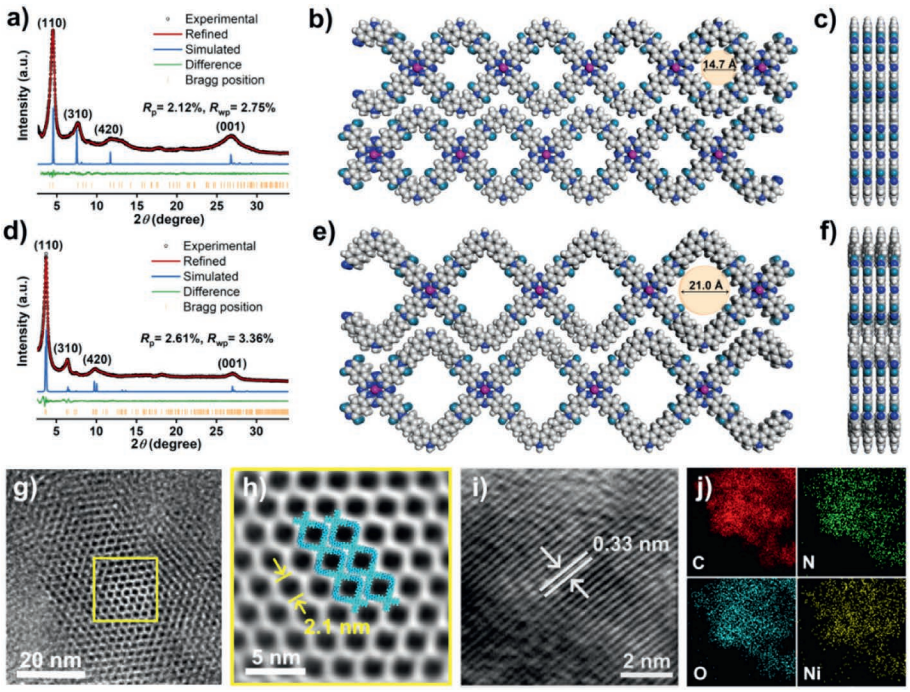


Fig. 1. PXRD patterns of (a) NiPc-CZDM-COF and (d) NiPc-CZDL-COF. Simulated structures of (b, c) NiPc-CZDM-COF and (e, f) NiPc-CZDL-COF (C: grey; N: blue; O: cyan; Ni: pink; H: white). (g-i) HRTEM images of NiPc-CZDL-COF. (j) EDS mapping photos of NiPc-CZDL-COF.

and Ni elements can be observed in the element energy dispersive spectroscopy (EDS) mapping, inferring the equably distributed metal active sites in two COFs (Fig. 1j and Fig. S14 in Supporting information).

The N_2 sorption measurements at 77 K reveal the moderate Brunauer-Emmett-Teller (BET) surface area of 85.7 and 57.3 m^2/g for NiPc-CZDM-COF and NiPc-CZDL-COF, respectively (Fig. S15 in Supporting information). As shown in Fig. S16 (Supporting information), the pore sizes concentrated on 1.49 and 2.13 nm have been determined for these two 1D COFs, in good agreement with the theoretical ones obtained from the structural models. The chemical stability of the two 1D COFs was assessed by soaking their samples into various solvents including N,N-dimethylformamide, tetrahydrofuran, 0.5 mol/L K_2SO_4, water, concentrated HCl, and ethanol, respectively, for 7 days. Fortunately, the crystalline structures remain well according to their consistent PXRD patterns to the fresh samples (Figs. S17 and S18 in Supporting information), indicating their good chemical stability.

X-ray photoelectron spectroscopy was measured to further characterize these two COFs. As shown in Figs. S19a and S20a (Supporting information), the binding energies of 872.68 (Ni $2p_{1/2}$) and 855.17 eV (Ni $2p_{3/2}$) for NiPc-CZDM-COF and 871.98 (Ni $2p_{1/2}$) and 855.01 eV (Ni $2p_{3/2}$) for NiPc-CZDL-COF manifest their divalent nickel nature. The chemical state and local coordination environment of Ni atoms were further studied by X-ray absorption near edge structure (XANES) spectroscopy. As exhibited in the Ni K-edge XANES spectra (Fig. 2a), the absorption edges of NiPc-CZDM-COF and NiPc-CZDL-COF are similar to those for commercial NiPc, further confirming the Ni^{2+} state in these two COFs. Fourier-transformed extended X-ray absorption fine structure (FT-EXAFS) spectra reveal that both COFs display Ni-N_4 scattering path peaks at 1.4 Å, consisted with commercial NiPc (Fig. 2b). In addition, EXAFS fitting results match well with their simulated structures (Fig. 2c and Fig. S21 in Supporting information). Similar results can be found in Wavelet transform (WT)-EXAFS with the Ni-N_4 scattering paths for NiPc-CZDM-COF and NiPc-CZDL-COF (Fig. 2d, Figs. S22 and S23 in Supporting information). These results demonstrate the consistency of the local coordination environment of COFs with commercial NiPc.

In consideration of the outstanding electrocatalytic performance of the molecular phthalocyaninato species and high utilization efficiency of the exposed active centers on the edges of 1D COFs, these two 1D NiPc-based COFs were expected to act as promising candidate for promoting electrocatalytic NO_3RR. The electrocatalytic capacity of two COFs was assessed in an H-type cell. The ink composed of COFs samples (1.0 mg) and Ketjen carbon black (1.0 mg) was spread on fiber paper (1 cm × 1 cm), which was used as working electrodes. The electrolyte containing 0.5 mol/L K_2SO_4

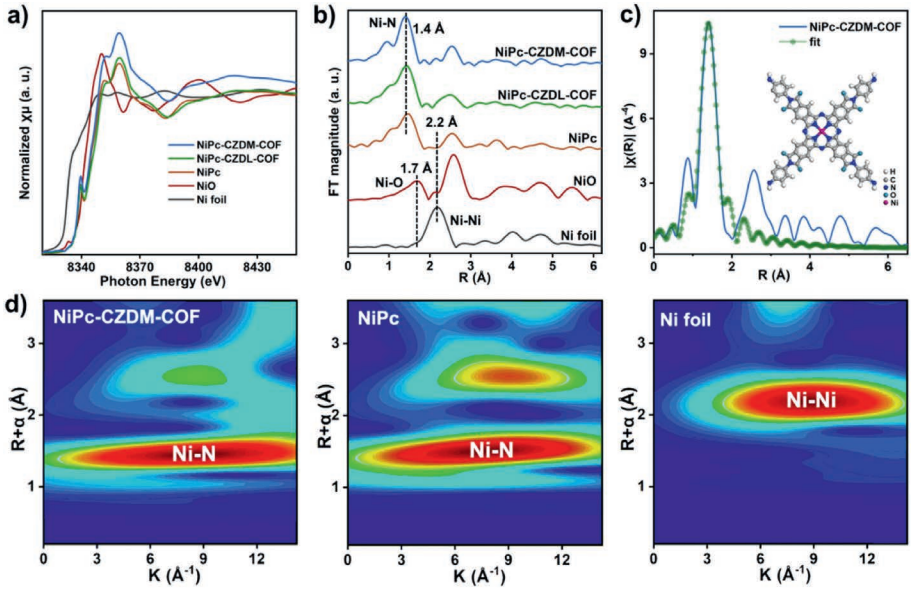


Fig. 2. (a) Ni K-edge XANES and (b) FT-EXAFS spectra of NiPc-CZDM-COF, NiPc-CZDL-COF, NiPc, NiO and Ni foil. (c) EXAFS fitting curves of Ni for NiPc-CZDM-COF. Inset: partial schematic structure of NiPc-CZDM-COF. (d) WT-EXAFS plots for Ni element of NiPc-CZDM-COF, NiPc and Ni foil.

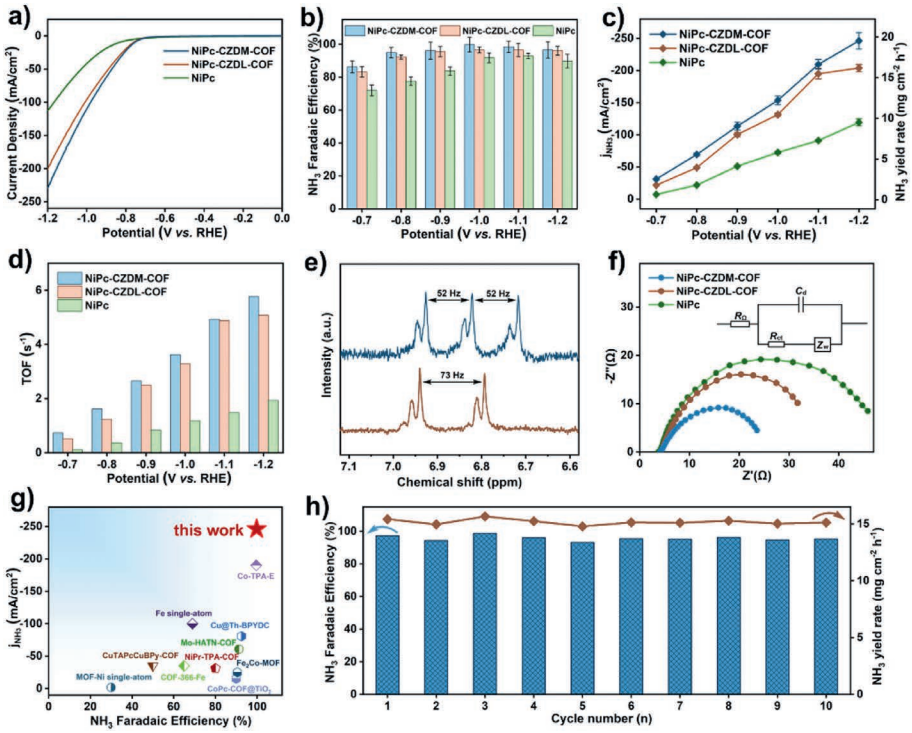


Fig. 3. (a) LSV curves, (b) FE_{NH_3}, (c) j_{NH_3} and NH_3 yield rate, (d) TOF of the two COF and NiPc. (e) ^1H NMR spectra of electrolyte after using $K^{14}NO_3$ and $K^{15}NO_3$ as the nitrogen source. (f) Nyquist plots of NiPc-CZDM-COF, NiPc-CZDL-COF and NiPc. (g) Comparison of FE_{NH_3} and j_{NH_3} with other reported catalysts. (h) Cyclic electrocatalytic test of NiPc-CZDM-COF.

and 0.1 mol/L KNO_3 was saturated with Ar for 20 min prior to measurement to eliminate the distraction of dissolved O_2. As displayed in the linear sweep voltammetry (LSV) curves measured in ambient conditions (Fig. 3a), the current densities of NiPc-CZDM-COF were much larger than NiPc-CZDL-COF, inferring the superior electrocatalytic activity of the former one. The production of NH_3 was measured using the indophenol blue method according to the UV–vis spectrophotometry (Fig. S24 in Supporting information). The quantification of NO_2^- was measured on the basis of the reported Griess test method (Fig. S25 in Supporting information) [62]. A spot of gaseous H_2 was detected by gas chromatograph (GC) monitoring. It is worth mentioning that no N_2H_4 and NH_2OH was detected in this electrocatalytic process according to UV–vis spectrophotometry (Figs. S26 and S27 in Supporting information).

Chronoamperometric (*i*–*t*) analysis was carried out at the potentials range from −0.7 V to −1.2 V to analyze the electrocatalytic products of NiPc-CZDM-COF, NiPc-CZDL-COF, and commercial NiPc (Figs. S28-S30 in Supporting information). As depicted in Fig. 3b and Figs. S31-S33 (Supporting information), NiPc-CZDM-

COF exhibits higher FE_{NH_3} of 86.3 %, 94.9 %, 96.1 %, 99.8 %, 98.4 %, and 96.6 % at −0.7, −0.8, −0.9, −1.0, −1.1, and −1.2 V accompanied by negligible H_2 and NO_2^- production in the system than that of 83.3 %, 92.3 %, 95.6 %, 96.6 %, 96.6 %, and 96.2 % for NiPc-CZDL-COF under the same condition, indicating the superior electrocatalytic activity of the former COF to the latter one. By contrast, commercial NiPc shows relatively lower FE_{NH_3} and obvious competitive hydrogen evolution reaction, inferring the structural superiority of the 1D COFs toward this electrocatalytic process. Additionally, NiPc-CZDM-COF shows larger j_{NH_3} of −31.1, −69.3, −113.4, −153.6, −209.7, and −246.2 mA/cm^2 at the potentials of −0.7, −0.8, −0.9, −1.0, −1.1, and −1.2 V than that of −21.6, −48.9, −100.3, −131.4, −195.1, and −203.4 mA/cm^2 for NiPc-CZDL-COF, and −7.2, −21.7, −51.1, −72.5, −91.1, and −119.3 mA/cm^2 for commercial NiPc at the same potentials (Fig. 3c). Notably, NiPc-CZDM-COF displays the record-breaking FE_{NH_3} and j_{NH_3} (100 % and −246 mA/cm^2) at −1.2 V among all the MOFs- and COFs-based electrocatalysts reported thus far (Fig. 3g and Table S1 in Supporting information). The NH_3 yield rates and turnover frequency (TOF) were calculated to be 19.5 mg cm^{-2} h^{-1} and 5.8 s^{-1} for NiPc-CZDM-COF, 16.2 mg cm^{-2} h^{-1} and 5.1 s^{-1} for NiPc-CZDL-COF, and 9.4 mg cm^{-2} h^{-1} and 1.9 s^{-1} for commercial NiPc at −1.2 V (Fig. 3d). It is worth noting that the conversion of nitrate in wastewater is significant. When the measurement was executed in the solution of 0.5 mol/L K_2SO_4 and 1000 ppm KNO_3, the FE_{NH_3} of NiPc-CZDM-COF exceeded 90 % over a wide voltage range of −0.8∼−1.2 V (Fig. S34 in Supporting information). Specifically, the sample exhibit j_{NH_3} of −127.2 mA/cm^2 and an impressive FE_{NH_3} of 98.5 % at −1.2 V, disclosing their good potential.

The surface concentration of available electrocatalytic active sites on the electrode was calculated to be 5.52×10^{-8} and 5.18×10^{-8} mol/cm^2 for NiPc-CZDM-COF and NiPc-CZDL-COF (Figs. S35-S37 in Supporting information), amounting to 8.03 % and 7.54 % of total NiPc in NiPc-CZDM-COF and NiPc-CZDL-COF, respectively, which in turn results in the excellent electrocatalytic capacity of these two COFs. The similar high ratio utilization efficiency of the electrocatalytic active sites actually comes from the ample active sites exposed on the edge sites of porous ribbons containing finite 1D chains for these two isostructural 1D COFs. Current-voltage curves reveal that NiPc-CZDM-COF displays a high conductivity of 2.05×10^{-3} S/m, 19 times higher than that of NiPc-CZDL-COF (1.07×10^{-4} S/m), leading to the more efficient electron transport of NiPc-CZDM-COF (Fig. S38 in Supporting information). Additional evidence can be gained from the electrochemical impedance spectroscopy (EIS) measurements. As shown in Fig. 3f, NiPc-CZDM-COF exhibits a much smaller charge transfer resistance than that of NiPc-CZDL-COF, inferring the preponderance of chemical dynamics of NiPc-CZDM-COF in this electrocatalytic process. As a consequence, NiPc-CZDM-COF unfolds the superior electrocatalytic performance to NiPc-CZDL-COF.

For the sake of determining the nitrogen source of NH_3 generated during the electrocatalytic NO_3RR process, a comparative experiment was carried out with only 0.5 mol/L K_2SO_4 solution as electrolyte under the same experimental condition. Negligible NH_3 was detected in the electrolyte for NiPc-CZDM-COF, announcing the nitrogen source of KNO_3 (Fig. S39 in Supporting information). Additional evidence for this point comes from the ^{15}N labeled isotopic experiment. As shown in Fig. 3e, the ^1H NMR spectrum exhibits typical two double peaks of $^{15}NH_3$ sitting at 6.94/6.93 and 6.81/6.79 ppm with the coupling constant of 73 Hz when using the solution of 0.5 mol/L K_2SO_4 and 0.1 mol/L $K^{15}NO_3$ as electrolyte. However, ^1H NMR spectrum shows three characteristic double peaks sitting at 6.94/6.93, 6.84/6.82, and 6.74/6.72 ppm with the coupling constant of 52 Hz for $^{14}NH_3$ when the electrolyte was replaced with the solution of 0.5 mol/L K_2SO_4 and 0.1 mol/L $K^{14}NO_3$. These results confirm the nitrogen source of NH_3 from

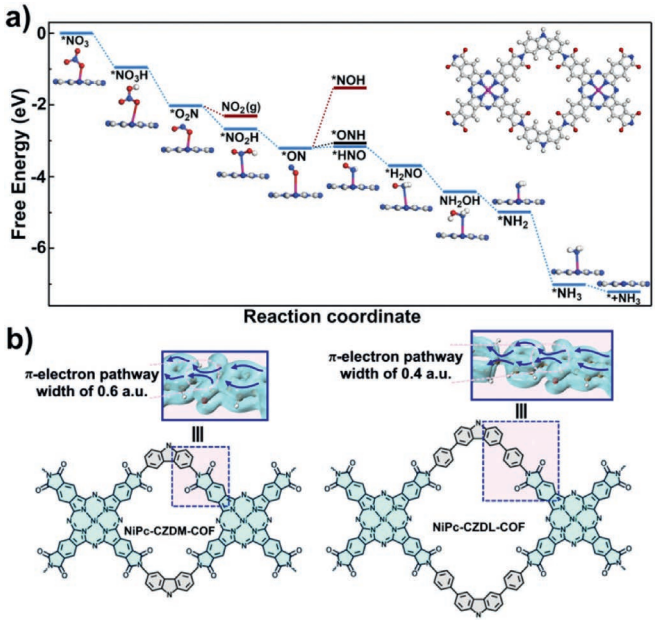


Fig. 4. (a) Energy pathway towards the NO_3RR for NiPc-CZDM-COF. (b) The π-electron pathways of NiPc-CZDM-COF and NiPc-CZDL-COF evaluated by the π-Mayer bond order theory.

KNO_3 in electrolyte rather than potential nitrogen pollution from catalysts and other external environments.

Electrocatalytic cyclic test experiment for NiPc-CZDM-COF and NiPc-CZDL-COF at a constant current of −200 mA was executed to evaluate its electrocatalytic stability. The electrolyte was gathered and analyzed to confirm electrocatalytic products per 30 min. The FE_{NH_3} of two COFs are higher than 92 % in every cycle accompanied by the almost non-attenuated NH_3 yield in the whole catalytic cyclic experiment, disclosing their good electrocatalytic stability (Fig. 3h and Fig. S41 in Supporting information). After the electrocatalytic cycles measurement, the NiPc-CZDM-COF on the cathode was characterized by PXRD, FT-IR, XPS spectroscopies, TEM and SEM images (Figs. S42-S45 in Supporting information). Notably, the PXRD pattern after electrocatalytic cyclic test agrees well with the fresh sample, indicating the maintained crystalline structure. The consistent FT-IR curves before and after electrocatalytic cyclic test also reveal the good structural durability. As shown in Fig. S44b, the high-resolution Ni 2p XPS spectra of NiPc-CZDM-COF after electrocatalytic cyclic test reveal unchanged divalent nickel nature with the binding energies of 872.25 (Ni $2p_{1/2}$) and 855.03 eV (Ni $2p_{3/2}$). As a consequence, the phthalocyanine-based imide-linked 1D COFs have outstanding durability in electrocatalysis.

Density functional theory (DFT) calculations were executed in order to clarify the electrochemical NO_3RR mechanism [63–65]. According to the DFT calculation results, the Gibbs free energy diagram of the eight electrons reducing pathway from nitrate to ammonia for NiPc-CZDM-COF, NiPc-CZDL-COF, and commercial NiPc were depicted in Fig. 4a and Figs. S46-S48 (Supporting information). In this pathway, the $*NO_3$ is dissociated to $*NO_2$ and then subsequent to *NO. The *NO in turn experiences the process of three proton-coupled electron transfers and forms $*NH_2OH$ followed by its reduction to NH_3 with its leaving from the catalyst surface as the end of one cycle. It is worth noting that the Gibbs free energy changing chains for these three samples are similar to each other, indicating the maintained electrocatalytic NO_3RR capacity of NiPc in the two NiPc-based 1D COFs.

Efficient charge transportation is crucial for electrocatalysis [66]. For NiPc, the electrons transportation relies mainly on the intermolecular e^- jumping between adjacent NiPc molecules [67],

which is much more difficult than that through the covalent bonds between NiPc and CZDM/CZDM, in turn resulting in the superior electrocatalytic NO_3RR performance of two 1D COFs to NiPc molecules. In addition, as shown in the π-electron pathways of NiPc-CZDM-COF and NiPc-CZDL-COF assessed according to the π-localized orbital locator (π-LOL) and π-Mayer bond order (π-MBO) theories (Fig. 4b) [68], the C–N bonds between imide moiety and CDZM unit provide much smoother electron transferring routes along with the larger π-electron flowing width of ~0.6 a.u. than that of ~0.4 a.u. afforded by the C–N bonds between imide moiety and CZDL unit, indicating the much more efficient charge transportation of NiPc-CZDM-COF than NiPc-CZDL-COF, in line with the experimentally revealed higher conductivity of NiPc-CZDM-COF. This supports the superior electrocatalytic activity of NiPc-CZDM-COF electrode. Additional evidence to stand this point comes from the calculated π-electronic coupling constants (π-ECC) of these two COFs [60]. The π-ECC for hole/electron transfer between double-layered NiPc for NiPc-CZDM-COF is 878/469 meV, much larger than those for NiPc-CZDL-COF, 592/211 meV (Table S4 in Supporting information). These results disclose the much more efficient charge transportation, higher conductivity, and superior electrocatalytic performance towards NO_3RR of NiPc-CZDM-COF than NiPc-CZDL-COF.

In summary, two novel 1D COFs with phthalocyanine building blocks and imide linkage have been synthesized. The high utilization and high electroactivity of exposed electroactive sites on the edge sites of these 1D COFs enable their efficient electrocatalysis performance for NO_3RR. In particular, NiPc-CZDM-COF exhibits superior electrocatalytic performance in terms of FE_{NH_3}, j_{NH_3}, NH_3 yield rate, and TOF to all the MOFs- and COFs-based catalysts reported thus far. This result not only provides an example on engineering 1D COFs-based electrocatalysts toward NO_3RR but also broadens the scope of 1D COFs with diverse application potentials.

Declaration of competing interest

The authors declare that they have no known competing financial interests or personal relationships that could have appeared to influence the work reported in this paper.

CRediT authorship contribution statement

Mingrun Li: Writing – original draft, Methodology, Data curation, Conceptualization. **Bin Han:** Writing – review & editing, Supervision, Data curation, Conceptualization. **Lei Gong:** Visualization, Software. **Yucheng Jin:** Visualization, Software. **Mingyue Wang:** Formal analysis, Data curation. **Xu Ding:** Software, Data curation. **Dongdong Qi:** Supervision, Software. **Jianzhuang Jiang:** Writing – review & editing, Supervision, Methodology, Conceptualization.

Acknowledgments

This work was financially supported by the Natural Science Foundation (NSF) of China (Nos. 22205015, 22175020, and 22235001), the National Postdoctoral Program for Innovative Talents (No. BX20220032), the China Postdoctoral Science Foundation Funded Project (No. 2022BG013), the Fundamental Research Funds for the Central Universities (Nos. 00007709, 00007770, and FRF-BR-23-02B), University of Science and Technology Beijing is gratefully acknowledged.

Supplementary materials

Supplementary material associated with this article can be found, in the online version, at doi:10.1016/j.cclet.2024.110590.

References

[1] Z. Wang, S. Zhang, Y. Chen, et al., Chem. Soc. Rev. 49 (2020) 708–735.
[2] C.S. Diercks, O.M. Yaghi, Science 355 (2017) eaal1585.
[3] Z.B. Zhou, H.H. Sun, Q.Y. Qi, et al., Angew. Chem. Int. Ed. 62 (2023) e202305131.
[4] X. Xu, X. Wu, K. Xu, et al., Nat. Commun. 14 (2023) 3360.
[5] X. Liu, X. Yang, X. Ding, et al., Chin. Chem. Lett. 34 (2023) 108148.
[6] Z. Liu, X. Yang, K. Wang, et al., Energy Storage Mater. 68 (2024) 103337.
[7] Y. Yang, D. Sabaghi, C. Liu, et al., Angew. Chem. Int. Ed. 63 (2024) e202316299.
[8] X. Yang, L. Gong, K. Wang, et al., Adv. Mater. 34 (2022) 2207245.
[9] R. Li, G. Xing, H. Li, et al., Chin. Chem. Lett. 34 (2023) 107454.
[10] K. Geng, T. He, R. Liu, et al., Chem. Rev. 120 (2020) 8814–8933.
[11] N. Li, C. Pan, G. Lu, et al., Adv. Mater. 36 (2024) 2311023.
[12] S. Suleman, Y. Zhang, Y. Qian, et al., Angew. Chem. Int. Ed. 63 (2024) e202314988.
[13] S. Lin, C.S. Diercks, Y.B. Zhang, et al., Science 349 (2015) 1208–1213.
[14] Q.J. Wu, D.H. Si, S. Ye, et al., J. Am. Chem. Soc. 145 (2023) 19856–19865.
[15] J.N. Chang, Q. Li, J.W. Shi, et al., Angew. Chem. Int. Ed. 135 (2023) e202218868.
[16] S. Bag, H.S. Sasmal, S.P. Chaudhary, et al., J. Am. Chem. Soc. 145 (2023) 1649–1659.
[17] Y. Cheng, J. Xin, L. Xiao, et al., J. Am. Chem. Soc. 145 (2023) 18737–18741.
[18] X. Wang, X. Ding, Y. Jin, et al., Angew. Chem. Int. Ed. 62 (2023) e202302808.
[19] Y. Xu, T. Sun, T. Zeng, et al., Nat. Commun. 14 (2023) 4215.
[20] B. Yu, R.B. Lin, G. Xu, et al., Nat. Chem. 16 (2024) 114–121.
[21] X. Han, C. Yuan, B. Hou, et al., Chem. Soc. Rev. 49 (2020) 6248–6272.
[22] J. Han, J. Feng, J. Kang, et al., Science 383 (2024) 1014–1019.
[23] Q. Guan, L.L. Zhou, Y.B. Dong, Chem. Soc. Rev. 51 (2022) 6307–6416.
[24] X. Wang, M. Bahri, Z. Fu, et al., J. Am. Chem. Soc. 143 (2021) 15011–15016.
[25] C. Qian, L. Feng, W.L. Teo, et al., Nat. Rev. Chem. 6 (2022) 881–898.
[26] B. Bishop, S. Huang, H. Chen, et al., Chin. Chem. Lett. 35 (2024) 109966.
[27] A. Natraj, W. Ji, J. Xin, et al., J. Am. Chem. Soc. 144 (2022) 9813–19824.
[28] H.L. Nguyen, C. Gropp, O.M. Yaghi, J. Am. Chem. Soc. 142 (2020) 2771–2776.
[29] Z. Chen, K. Wang, Y. Tang, et al., Angew. Chem. Int. Ed. 62 (2023) e202213268.
[30] H.S. Xu, Y. Luo, X. Li, et al., Nat. Commun. 11 (2020) 1434.
[31] L. Zou, Z.A. Chen, D.H. Si, et al., Angew. Chem. Int. Ed. 62 (2023) e202309820.
[32] S. An, X. Li, S. Shang, et al., Angew. Chem. Int. Ed. 62 (2023) e202218742.
[33] S. Qiao, J. Wang, Z. Guo, et al., Inorg. Chem. 63 (2024) 706–713.
[34] C. Jia, A. Duan, C. Liu, et al., Small 19 (2023) 2300518.
[35] P.L. Holland, Chem. Rev. 120 (2020) 4919–4920.
[36] Q. Hu, K. Yang, O. Peng, et al., J. Am. Chem. Soc. 146 (2024) 668–676.
[37] W. Guo, K. Zhang, Z. Liang, et al., Chem. Soc. Rev. 48 (2019) 5658–5716.
[38] Y. Pang, C. Su, G. Jia, et al., Chem. Soc. Rev. 50 (2021) 12744–12787.
[39] P. Xu, G. Li, Y. Zheng, et al., Nature 626 (2024) 792–798.
[40] J. Miao, Q. Hong, L. Liang, et al., Chin. Chem. Lett. 35 (2024) 108935.
[41] L. Liu, S.J. Zheng, H. Chen, et al., Angew. Chem. Int. Ed. 63 (2024) e202316910.
[42] Y. Wang, F. Hao, M. Sun, et al., Adv. Mater. 36 (2024) 2313548.
[43] Y. Chen, X. Xia, L. Tian, et al., Chin. Chem. Lett. 35 (2024) 109789.
[44] M. Xie, S. Tang, Z. Li, et al., J. Am. Chem. Soc. 145 (2023) 13957–13967.
[45] Y. Lv, S.W. Ke, Y. Gu, et al., Angew. Chem. Int. Ed. 62 (2023) e202305246.
[46] R. Liu, K.T. Tan, Y. Gong, et al., Chem. Soc. Rev. 50 (2021) 120–242.
[47] G. Cai, P. Yan, L. Zhang, et al., Chem. Rev. 121 (2021) 12278–12326.
[48] B. Han, Y. Jin, B. Chen, et al., Angew. Chem. Int. Ed. 61 (2022) e202114244.
[49] M. Li, B. Han, S. Li, et al., Small 20 (2024) 2310147.
[50] H. Guo, D.H. Si, H.J. Zhu, et al., Angew. Chem. Int. Ed. 63 (2024) e202319472.
[51] H. Liu, J. Chu, Z. Yin, et al., Chem 4 (2018) 1696–1709.
[52] Q. Zhi, R. Jiang, X. Yang, et al., Nat. Commun. 15 (2024) 678.
[53] M. Liu, S. Yang, S. Liu, et al., Small 18 (2022) 2204757.
[54] X. Zhao, P. Pachfule, A. Thomas, Chem. Soc. Rev. 50 (2021) 6871–6913.
[55] M. Martínez-Fernández, E. Martínez-Periñán, A. de la Peña Ruigómez, et al., Angew. Chem. Int. Ed. 62 (2023) e202313940.
[56] J. Liu, J. Zhao, C. Li, et al., Small 20 (2024) 2305759.
[57] F. Lv, M. Sun, Y. Hu, et al., Energy Environ. Sci. 16 (2023) 201–209.
[58] H. Hu, R. Miao, F. Yang, et al., Adv. Energy Mater. 14 (2024) 2302608.
[59] H. Huang, K. Wang, Green Chem. 25 (2023) 9167–9174.
[60] B. Han, X. Ding, B. Yu, et al., J. Am. Chem. Soc. 143 (2021) 7104–7113.
[61] Q. Fang, Z. Zhuang, S. Gu, et al., Nat. Commun. 5 (2014) 4503.
[62] Y. Wu, Z. Jiang, Z. Lin, et al., Nat. Sustain. 4 (2021) 725–730.
[63] T.S. Bui, E.C. Lovell, R. Daiyan, et al., Adv. Mater. 35 (2023) 2205814.
[64] T. Hu, C. Wang, M. Wang, et al., ACS Catal. 11 (2021) 14417–14427.
[65] Y. Xiong, Y. Wang, J. Zhou, et al., Adv. Mater. 35 (2023) 2304021.
[66] C. Wang, Z. Lv, W. Yang, et al., Chem. Soc. Rev. 52 (2023) 1382–1427.
[67] S. Senthilarasu, R. Sathyamoorthy, J.A. Ascencio, et al., J. Appl. Phys. 101 (2007) 034111.
[68] J. Du, J. Hurd, J.A. Seed, et al., J. Am. Chem. Soc. 145 (2023) 21766–21784.